Non-Orthogonal Modulation for Short Packets in Massive Machine Type Communications

Chin-Wei Hsu, Hun-Seok Kim, *Member, IEEE*
Department of EECS, University of Michigan, Ann Arbor, MI
chinweih@umich.edu, hunseok@umich.edu

GLOBECOM 2020 - 2020 IEEE Global Communications Conference | 978-1-7281-8298-8/20/$31.00 ©2020 IEEE | DOI: 10.1109/GLOBECOM42002.2020.9348238

***Abstract*—Massive Machine Type Communication (mMTC) enables novel applications but its dense deployment and short packet properties lead to new challenges for physical layer design. This paper investigates hyper-dimensional modulation (HDM), a recently proposed novel non-orthogonal modulation, for short packet communications with superior interference tolerance in mMTC. We propose a new tree-based K-best decoding algorithm for HDM to improve the packet error rate performance in both additive white Gaussian noise (AWGN) and interference-limited scenarios. Simulation results show that the proposed algorithm can achieve 0.5 – 4 dB gain in AWGN and interference-limited channels compared to the Polar code with CRC (cyclic redundancy check)-aided list decoding.**

I. Introduction

The ITU-R categorizes the 5G and beyond technologies into three classes: enhanced Mobile Broadband (eMBB), massive Machine Type Communications (mMTC), and Ultra-Reliable and Low Latency Communications (URLLC) while each targets different applications [1]. mMTC use-case examples include transportation, utilities, health, environment, and security [2]. Packets for these mMTC applications usually carry very small amount of information such as control commands or sensor readings. The number of nodes in mMTC networks can be much greater than that of consumer (non-machine) mobile cellular networks. Thus it poses new challenges in the physical layer (PHY) design for reliable communication of short packets in interference-heavy channels [3].

Up to 4G, the main focus of the development has been to boost the data rate with high spectral efficiency for human-oriented communications. However, novel applications in mMTC usually convey relative short information as small as a few bytes per packet. The conventional PHY and network design optimized for large amount of information is no longer efficient in those applications. First, the overhead of preamble and pilot symbols is no longer negligible compared to the small number of information bits. Therefore, the frame structure needs to be re-designed with consideration of the overhead [4]. Second, the efficiency of modern codes such as Turbo and LDPC codes greatly relies on the long block-length. When the packet size is small, these codes fail to provide reliable performance. A new theorem has been studied to provide the limit of short codes since Shannon's Theorem assumes infinite block-length [5]. To approach the limit for short codes, new coding schemes have been recently investigated [6], [7].

Another challenge in mMTC is the interference especially when it operates in unlicensed ISM bands. Grant-based multiple access protocols are inefficient when the number of nodes is large [3]. The overhead of control signals for network coordination often offsets the potential benefits of being synchronous. Moreover, precise synchronization in time and frequency is impractical for many very narrowband low power mMTC nodes because of frequency reference oscillator-accuracy limitations and the energy burden of maintaining synchronization even when there is no message to communicate. When an asynchronous mMTC network operates in unlicensed band shared with heterogeneous systems such as WiFi, Bluetooth, etc., inter-/intra-network collisions and interference become inevitable. Therefore, it is a critical task for mMTC to design a novel PHY for short packets to deal with overwhelming interference from both intra- and heterogeneous inter-network traffics.

Hyper-Dimensional Modulation (HDM) is a novel non-orthogonal modulation proposed recently [8], [9]. It was shown that HDM can provide excellent reliability when the packet length is short and it is inherently tolerate to interference. Therefore, HDM has great potential for adoption in mMTC systems. Originally HDM was proposed with a demodulation algorithm using an iterative parallel successive interference cancellation (SIC) technique [8]. It then be extended to use the knowledge of intra-network interference to improve the performance under packet collisions [9]. In this paper, we proposed a new demodulation algorithm to further improve the performance of HDM in AWGN and interference-limited channels outperforming the state-of-the-art CRC-assisted list-decoding based Polar code [10] applied to binary phase-shift keying (BPSK) for the same spectral efficiency and coding rate.

Several prior works have investigated the PHY design for short packet communications and mMTC. The performance and complexity comparison for modern codes are provided in [11]. However, the comparison is only valid in the AWGN channel (without interference). Grant-free (with interference collision) NOMA performance for mMTC is analyzed in [12]. However, the system still needs to be synchronized to a time reference for a slot-based multiple access scheme. A compressive sensing based modulation is proposed for mMTC in [13]. However, the proposed joint multi-user decoding only works for synchronous systems and can not deal with heterogeneous interference sources. In contrast, our approach is designed for asynchronous short packet systems that coexist with interference from heterogeneous systems. Three main contributions

of this paper can be summarized as: 1) a new tree-based CRC-assisted K-best decoding to significantly improve the performance of HDM for short packets, 2) formulation of L1 optimization decoding for enhanced interference tolerance, and 3) evaluation of the proposed HDM and new algorithms to outperform the Polar-coded BPSK for the same spectral efficiency and coding rate under strong interference.

II. System Model

Hyper-Dimensional Modulation (HDM) is a novel non-orthogonal modulation recently proposed for short packet communications [8]. HDM can be viewed as a *joint modulation-coding* method and a special case of superposition codes [14] which construct the modulated (and coded) signal by combining selected columns of a random codebook. Instead of using a random codebook as in typical superposition codes, HDM uses a fast linear transform and pseudo-random permutations to transform sparse vectors to non-sparse vectors for efficient encoding and decoding. The HDM modulation process can be written as

$$\mathbf{s} = \sum_{i=1}^{V} \mathbf{A}_i \mathbf{x}_i \tag{1}$$

where $\mathbf{s}$ denotes the complex-valued transmitted vector with dimension of $D \times 1$ ($\mathbf{s} \in \mathbb{C}^D$), $\mathbf{x} = [\mathbf{x}_1^T \ \mathbf{x}_2^T \ \cdots \ \mathbf{x}_V^T]^T$ and $\mathbf{A} = [\mathbf{A}_1 \ \mathbf{A}_2 \ \cdots \ \mathbf{A}_V]$ represent the composition of the sparse information vectors and the codebook, respectively. The information vectors $\mathbf{x}_i \in \mathbb{C}^D$ for $i = 1, \cdots, V$ are sparse with only one non-zero element and V is defined as the number of *non-orthogonal* layers that are transmitted at the same time. The sparse vector $\mathbf{x}_i$ embeds the information bits in the position of the non-zero element and the value (phase) of the non-zero element, which can be chosen from QPSK symbols: $\{+1, -1, +j, -j\}$. The matrix $\mathbf{A}_i \in \mathbb{C}^{D \times D}$ represents a fast linear transformation followed by a pseudo-random permutation. Thus, the transmitted signal is the superposition of V non-sparse vectors $\mathbf{A}_i\mathbf{x}_i$, which can be obtained by $\mathbf{A}_i\mathbf{x}_i = \mathbf{P}_i\mathcal{F}\{\mathbf{x}_i\}$ where $\mathbf{P}_i$ is a pseudo-random permutation matrix and $\mathcal{F}\{\cdot\}$ is a fast linear transform with complexity of $O(N \log N)$ (e.g., fast Fourier transform (FFT) or fast Walsh–Hadamard transform (FWHT)). Note that the matrix $\mathbf{A}_i$ is unitary if normalized, and vectors $\mathbf{A}_i\mathbf{x}_i$ are *non-orthogonal* although they are transmitted together.

Assuming a narrowband frequency flat channel and perfect channel estimation, the received signal $\mathbf{y}$ can be represented by (2) assuming the channel is equalized.

$$\mathbf{y} = \mathbf{s} + \mathbf{n} = \sum_{i=1}^{V} \mathbf{A}_i \mathbf{x}_i + \mathbf{n}. \tag{2}$$

In (2), $\mathbf{n} \sim \mathcal{CN}(0, N_0\mathbf{I})$ is the complex Gaussian noise vector with element-wise variance N_0. The demodulation process in AWGN can be considered as finding the optimal solution of the non-convex minimization problem:

$$\text{P1: } \arg\min_{\mathbf{x} \in \mathcal{X}} \|\mathbf{y} - \sum_{i=1}^{V} \mathbf{A}_i \mathbf{x}_i\|_2^2 \tag{3}$$

where $\mathcal{X}$ represents the set of all possible sparse information vectors $\mathbf{x}_i$ (i.e., each $\mathbf{x}_i$ contains only one non-zero QPSK symbol encoding $\log_2 D + 2$ bits by the position and phase).

This problem resembles compressive sensing, which finds the optimal sparse vector with minimum L1-norm that satisfies an L2-norm constraint. However, compressive sensing is usually a convex problem which has a solution in a convex set of sparse vectors, whereas the problem in (3) is non-convex because of the constraint on the discrete and non-convex set $\mathcal{X}$. Next, we discuss an efficient K-best tree-search method to solve the problem, which yields lower error rate compared to our prior parallel-SIC decoding [8], [9].

III. K-best Decoding Algorithm

A bruteforce method to find the minimum of (3) by trying all possible combinations of $\mathbf{x}_i, i = 1, \cdots, V$ is practically infeasible due to excessive complexity. Therefore, in this section we propose a tree-based algorithm that finds a suboptimal solution of (3) through a K-best breath-first search algorithm similar to a variant in MIMO decoding [15].

First observe that the objective in (3) can be expressed as

$$\begin{aligned}\|\mathbf{y} - \sum_{i=1}^{V} \mathbf{A}_i \mathbf{x}_i\|_2^2 = \|\mathbf{y} - \sum_{i=1}^{V-1} \mathbf{A}_i \mathbf{x}_i\|_2^2 + \|\mathbf{A}_V \mathbf{x}_V\|_2^2 \\ - 2\Re\{\mathbf{y}^H \mathbf{A}_V \mathbf{x}_V\} + 2\Re\{(\sum_{i=1}^{V-1} \mathbf{A}_i \mathbf{x}_i)^H \mathbf{A}_V \mathbf{x}_V)\}\end{aligned} \tag{4}$$

where $\Re\{\cdot\}$ denotes the real part of a complex number.

In (4), the norm in right-hand side (RHS) consists of four terms. The first term $\|\mathbf{y} - \sum_{i=1}^{V-1} \mathbf{A}_i \mathbf{x}_i\|_2^2$ has the same form as LHS except the summation is now from 1 to $V-1$. The second term $\|\mathbf{A}_V \mathbf{x}_V\|_2^2$ is a constant regardless of the choice of $\mathbf{x}_V$ if the fast linear transformation matrix has columns with equal norms. The third term is the correlation between $\mathbf{y}$ and $\mathbf{A}_V\mathbf{x}_V$. Finally, the last term is the correlation between $\mathbf{A}_V\mathbf{x}_V$ and an accumulative vector $\sum_{i=1}^{V-1} \mathbf{A}_i\mathbf{x}_i$. With the same process, the first term in RHS can be further decomposed until only $\mathbf{y}$ remains.

Subtract the objective function in (3) by constant terms $\|\mathbf{A}_i\mathbf{x}_i\|_2^2$ for $i = 1, \cdots, V$ and divide the equation by 2, then the solution of the minimization problem remains identical. Therefore, we can denote the *score metric* $s^{(l)} = \frac{1}{2}(\|\mathbf{y} - \sum_{i=1}^{l} \mathbf{A}_i\mathbf{x}_i\|_2^2 - \sum_{i=1}^{l} \|\mathbf{A}_i\mathbf{x}_i\|_2^2)$, which can be expressed in an iterative form:

$$s^{(l)} = s^{(l-1)} - \Re\{\mathbf{x}_l^H \mathbf{A}_l^H \mathbf{y}\} + \Re\{\mathbf{x}_l^H \mathbf{A}_l^H \mathbf{u}^{(l-1)}\} \tag{5}$$

where $\mathbf{u}^{(l)} = \sum_{i=1}^{l} \mathbf{A}_i\mathbf{x}_i$.

The objective is to minimize (5) for the last layer V, $s^{(V)}$. Thus we find the minimum metric through a tree structure by evaluating sparse vectors $\mathbf{x}_l$ for each layer. Note that at each node of the tree, we calculate the metric (5) for each candidate

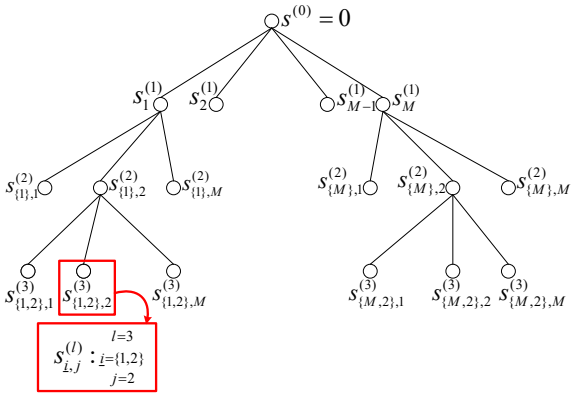

Fig. 1: The tree structure illustration of K-best algorithm. M is the number of candidates $\mathbf{x}_l$ at each layer, which equals to $4D$ when QPSK symbols are used. The layer indices have been sorted.

of $\mathbf{x}_l$ with fixed candidates determined by all previous layers from 1 to $l-1$ (*i.e.*, $s^{(l-1)}$ and $\mathbf{u}^{(l-1)}$).

The tree structure is illustrated in Fig. 1. For each parent node, we calculate its children's metric based on the parent's metric and also its ancestor path. More specifically, we can rewrite the iterative equation (5) for each node given its parent and ancestor path as

$$s_{\underline{i},j}^{(l)} = s_{\underline{i}}^{(l-1)} - \Re\{\mathbf{x}_{l,j}^H \mathbf{A}_l^H \mathbf{y}\} + \Re\{\mathbf{x}_{l,j}^H \mathbf{A}_l^H \mathbf{u}_{\underline{i}}^{(l-1)}\} \qquad (6)$$

where j is the j-th candidate of possible $\mathbf{x}_l$, and $\underline{i} = \{i_1, i_2, \cdots, i_{l-1}\}$ is the index set of previously chosen paths of its ancestor nodes. The accumulative vector $\mathbf{u}_{\underline{i}}^{(l-1)}$ is the interference term determined by previously chosen candidates from parent/ancestor layers.

The demodulation process follows a K-best tree structure searching algorithm. Without pruning, the number of nodes to traverse grows exponentially with the size of possible $\mathbf{x}$ candidates as we go deeper into the tree. To maintain practical complexity, we only preserve for each layer the best K candidates with lowest metrics and prune all the others. The iteration continues until there are K surviving nodes at the last layer eventually.

There are efficient ways to calculate the metric (6). Since only one element of $\mathbf{x}_l$ has the non-zero value which can only be a QPSK symbol, the last two terms of RHS in (6) is equivalent to simply choosing a single real and imaginary number from the elements of $\mathbf{A}_l^H\mathbf{y}$ and $\mathbf{A}_l^H\mathbf{u}_{\underline{i}}^{(l-1)}$, respectively. Furthermore, $\mathbf{A}_l^H\mathbf{y}$ can be computed by a fast linear transform followed by permutation (matrix–vector multiplication is not required), and $\mathbf{A}_l^H\mathbf{u}_{\underline{i}}^{(l-1)} = \sum_{j=1}^{l-1} \mathbf{A}_l^H\mathbf{A}_j\mathbf{x}_{j,i_j}$ can be obtained by summing columns of look up tables that store pre-computed $\mathbf{A}_l^H\mathbf{A}_j$ for $l = 1, \cdots, V$ and $j = 1, \cdots, l-1$. In this way, the computation complexity can be kept as $O(D \log D + K)$.

CRC-assisted error correction: A near-optimal solution is obtained by choosing the one with the lowest metric from the final output list. If K is sufficiently large, the suboptimal solution often gives the correct decoding result. The error probability can further decrease by checking CRC to determine whether the selected candidate is valid or not. Since we have a list of K best candidates, one can try each of them with the order of ascending metric until the candidate passes CRC. Even in the event that the set of correct vectors is not the optimal solution of (5), it is still highly probable to identify it as long as it is in the final candidate list.

Sorting-based K-best: One potential weakness of the K-best algorithm is that if a decision is made wrong in an upper layer, that mistake can not be recovered in lower layers. To mitigate this issue, we propose a strategy to sort the order of decoding layers based on the score metric along the tree traversal. We consider two possible methods for sorting the decoding layers; the first one is *universal* sorting and the second is *per-branch* sorting. For *universal* sorting, we first evaluate minimum metrics of all remaining layers based on (6) using the up-to-now best candidate as $\mathbf{u}$. Then we pick a layer with the best possible metric as the layer to be processed next for all (universal) K surviving nodes. The *per-branch* sorting method is similar to the *universal* method except that it uses different accumulative vectors $\mathbf{u}$ for each surviving nodes. Then each node can decide the order of next layer to decode, which may result in a different order from others. This method has higher complexity but yields better performance.

The entire demodulation algorithm using the *per-branch* sorting method is summarized in Algorithm 1. Converting it to the *universal* sorting method is straightforward.

Algorithm 1: K-best decoding algorithm with CRC correction and *per-branch* sorting method.

Input : $\mathbf{y}, K, \mathbf{P}_i$, for $i = 1, \cdots, V$
Output: decodedBits, errFlag

for $k = 1$ **to** K **do**
  $\mathbf{u}(k) \leftarrow 0$ (zero accumulative vector)
  $s(k) \leftarrow 0$ (zero score metric)
  $\mathsf{idx}(k) \leftarrow [\,]$ (empty candidate index)
  $\mathcal{L}(k) \leftarrow [\,]$ (empty decoded layer index)
for $i = 1$ **to** V **do**
  for $k = 1$ **to** K **do**
    $l_k \leftarrow \texttt{ChooseLayer}(\overline{\mathcal{L}(k)})$
    $\mathcal{L}(k) \leftarrow [\mathcal{L}(k), l_k]$
    $s^{tmp}(k) \leftarrow s(k) - \Re\{\mathcal{F}\{\mathbf{P}_{l_k}^H\mathbf{y}\}\} + \Re\{\mathcal{F}\{\mathbf{P}_{l_k}^H\mathbf{u}_k\}\}$
  $[\mathbf{s}, \mathsf{idx}_{new}, \mathsf{anc}] \leftarrow \texttt{SelectNodes}(s^{tmp}, K)$
  for $k = 1$ **to** K **do**
    $\mathbf{u}(k) \leftarrow \mathbf{u}(\mathsf{anc}(k)) + \mathbf{P}_{l_{\mathsf{anc}(k)}}\mathcal{F}\{\mathbf{x}_{\mathsf{idx}_{new}(k)}\}$
    $\mathsf{idx}(k) \leftarrow [\mathsf{idx}(\mathsf{anc}(k)), \mathsf{idx}_{new}(k)]$
outputList $\leftarrow \texttt{Reorder}(\mathsf{idx}, \mathcal{L})$
while errFlag $\neq 0$ *and* $k \leq K$ **do**
  decodedBits $\leftarrow \texttt{IdxToBits}(\mathsf{outputList}\ (k))$
  errFlag $\leftarrow \texttt{CRCDecode}(\mathsf{decodedBits})$

IV. Detection under Strong Interference

A. Modified formulation to mitigate interference

When there exists strong interference in the environment, the optimization P1 in (3) does not necessarily yield the optimal performance because interference may have time-varying power and does not behave as i.i.d. Gaussian noise throughout the packet. In our narrowband mMTC scenarios, interference burst length can be much shorter than the length of the desired packet, and multiple interference sources can overlap with each other with random arrival processes. In that scenario, it is reasonable to assume that the receiver does not know interference property such as the average/instantaneous power level and position of interference bursts within a desired packet. For example, when a narrowband mMTC system operates in the 2.4GHz ISM band, the gateway may observe heavy interference coming from WiFi and Bluetooth. A packet from WiFi or Bluetooth will be much shorter than a narrowband (e.g., a few kHz) mMTC packet while the interference power information is unknown and may change quickly.

Applying the decoding algorithm in section II in severe interference scenarios will result in suboptimal performance. Degradation comes from the possibility of sporadic interference causing *some* received samples having large Euclidean distance from the transmitted samples. These events can result in large L2-norm.

One technique to alleviate this problem is to set a saturation threshold on the received sample to prevent the large offset from the transmitted signal caused by the sporadic strong interference. Another strategy is to use an alternative metric to replace the L2-norm to handle the problem. We propose to use L1-norm as the metric because it is less sensitive to sporadic outlier elements in a large vector. The optimization in this case changes from L2- to L1-norm objective:

$$\text{P2: } \arg\min_{\mathbf{x}\in\mathcal{X}} \|\mathbf{y} - \sum_{i=1}^{V} \mathbf{A}_i\mathbf{x}_i\|_1. \tag{7}$$

B. K-best decoding with L1-norm metric

The L1-norm in (7) can not be decomposed in the same form as the L2-norm in (3) with iterative calculation. Nevertheless, if the vectors and matrices in (7) are real, i.e., $\mathbf{y}, \mathbf{x}_i \in \mathbb{R}^D$ for $i = 1, 2, \cdots, V$ and $\mathbf{A}_i \in \mathbb{R}^{D\times D}$ for $i = 1, 2, \cdots, V$, then (7) can have an iterative additive form.

Lemma 1. *If $a, b \in \mathbb{R}$, then $|a+b| = |a|+|b|-2\cdot\mathbb{1}(ab<0)\cdot\min(|a|,|b|)$, where $\mathbb{1}(\cdot)$ is the indicator function that equals to 1 if the condition in the parentheses is true or 0 otherwise.*

Using Lemma 1, we can decompose the L1-norm as

$$\|\mathbf{a}+\mathbf{b}\|_1 = \|\mathbf{a}\|_1 + \|\mathbf{b}\|_1 - 2\sum_{i=1}^{D} \mathbb{1}(a_i b_i < 0)\cdot\min(|a_i|,|b_i|) \tag{8}$$

where $\mathbf{a}$ and $\mathbf{b} \in \mathbb{R}^D$, and a_i denotes the i-th element of $\mathbf{a}$. Now, the objective function (7) is calculated iteratively as

$$\begin{aligned}\|\mathbf{y} - \sum_{i=1}^{V} \mathbf{A}_i\mathbf{x}_i\|_1 &= \|y - \sum_{i=1}^{V-1} \mathbf{A}_i\mathbf{x}_i\|_1 + \|\mathbf{A}_V\mathbf{x}_V\|_1 \\ &- 2\mathbf{1}^T\big(\mathbb{1}(\mathbf{r}_{V-1}\circ\mathbf{A}_V\mathbf{x}_V>0)\circ\min(|\mathbf{r}_{V-1}|,|\mathbf{A}_V\mathbf{x}_V|)\big)\end{aligned} \tag{9}$$

where $\mathbf{r}_{V-1} = \mathbf{y} - \sum_{i=1}^{V-1}\mathbf{A}_i\mathbf{x}_i$ and $\mathbf{1}$ is a vector with all elements of 1, and $\circ$ denotes element-wise multiplication. Note that the term $\|\mathbf{A}_V\mathbf{x}_V\|_1$ is a constant if $\mathbf{A}_V$ has constant L1-norm columns, which is true when FWHT is used instead of FFT. Hence, the iterative L1 calculation has the form:

$$s^{(l)} = s^{(l-1)} - \mathbf{1}^T\big(\mathbb{1}(\mathbf{r}_{l-1}\circ\mathbf{A}_l\mathbf{x}_l>0)\circ\min(|\mathbf{r}_{l-1}|,|\mathbf{A}_l\mathbf{x}_l|)\big). \tag{10}$$

The same K-best algorithm structure can be used with the L1 metric calculation (10). Note (10) does not involve matrix multiplications since $\mathbf{x}_l$ has only one non-zero element and the other terms are just choosing sign and magnitude values between two vectors.

C. Separate IQ modulation for L1 K-best

The aforementioned L1 formulation requires real-valued modulation. To maintain the same spectral efficiency with the original HDM that uses complex-valued QPSK and FFT, we use binary (±1) modulation for $\mathbf{x}_i$ and real-valued FWHT for $\mathbf{A}_i$ independently applied to the in-phase and quadrature (I and Q) channels. In that case, the K-best demodulation is performed separately with the I and Q channel of the signal. The CRC-correction stage needs to be modified because now we have two candidate lists. We evaluate possible candidate combinations for CRC using both lists while limiting the number of CRC trials to be linear with K.

V. Evaluation

A. Performance in AWGN

The performance of the proposed HDM is evaluated by Monte-Carlo simulations. We compare the proposed scheme with BPSK modulation protected by a 3GPP specified CRC-aided Polar code with a list decoding method [10], [16]. This Polar code configuration is known to be very robust for short-length codes [11]. For HDM, we use $D = 128, V = 7$, which gives a coding rate of 0.4922. We set $K = 128$ in our K-best decoding. With this setting the decoder needs only 5.25 MB for complex-valued look up tables for algorithm complexity reduction described in Section III. For Polar code, we set the coding rate to 0.5 and the decoding list size to 8. The decoding complexity of list decoder grows with the list size, and thus cannot be set too large for complexity concern. As a narrowband mMTC scenario, we assume a short packet that corresponds to a single $D = 128$ vector for HDM and a 128-bit codeword for BPSK-Polar. The coding rate of 0.5 means 64 information bits per packet. Both schemes use a 11-bit CRC for error correction assistance while the CRC bits are included in the information bits. Note that both HDM and

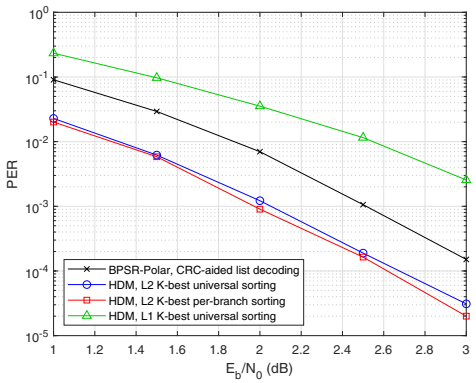

Fig. 2: PER of HDM vs. BPSK-Polar in AWGN.

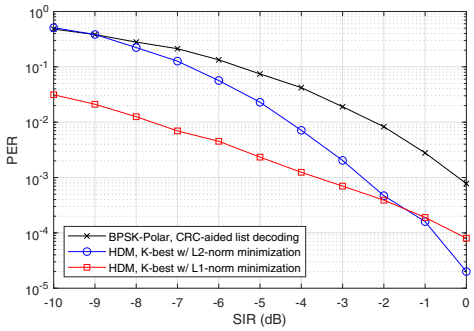

Fig. 3: PER of HDM vs. BPSK-Polar for various SIRs.

BPSK-Polar have the same spectral efficiency of 0.5 bit/s/Hz (0.4922 for HDM to be precise).

Figure 2 shows the packet error rate (PER) of HDM and Polar coded BPSK. One packet corresponds to a single transmit vector in HDM and a single codeword in BPSK-Polar. The HDM with L2 K-best decoding outperforms the BPSK-Polar by 0.5 dB while the *per-branch* sorting slightly outperforms the *universal* sorting for HDM. HDM with L1 K-best is expected to have worse performance because L1-norm is not a proper metric in this case without interference.

B. Performance with Strong Interference

In this subsection we consider a narrowband (1kHz) mMTC system coexists with wideband systems such as WiFi and Bluetooth. The interference comes from other systems whose packets follow a Poisson arrival process. Each interference packet is assumed to have a length of 2 ms (typical WiFi/Bluetooth packet) which is much shorter than the 1kHz-bandwidth HDM and BPSK-Polar packet length of 128 ms.

To model the random power distribution of interference packets, we consider an mMTC gateway receiver at the center of a circle where all interference transmitters are distributed following a spatial Poisson point process. The interference power attenuation due to the carrier frequency mismatch can be modeled as $\sim \frac{A}{\sigma\sqrt{2\pi}} e^{-\frac{\Delta f^2}{2\sigma^2}}$, where Δf is the carrier frequency mismatch, and A and σ are system dependent parameters [9]. In addition to the distance-dependent free-space pathloss, the interference power loss from shadowing is modeled as a log-normal distribution. Combining these models, the interference power (in dB) at the gateway is expressed as $P_{rx} = P_{tx} - c_1 \log(\mathcal{U}) - c_2(\mathcal{U})^2 + c_3\mathcal{N} + c_4$ where P_{tx} is the transmit power, c_1, c_2, c_3, c_4 are model constants, and $\mathcal{U}, \mathcal{N}$ denote unit variance uniform and normal random variables following $\mathcal{U}(0,1)$ and $\mathcal{N}(0,1)$, respectively. For a narrowband system with signal bandwidth of 1kHz, a reasonable model constants are $c_1 = 10$ and $c_2 = 11.8541$. Depending on the environment (macrocell / microcell / indoor) c_3 ranges from 4 to 13 [17]. By assuming that P_{tx} is fixed, the power distribution of interference packets at the gateway can be approximated as log-normal dominated by the term $c_3\mathcal{N}$.

Figure 3 shows the PER performance of different schemes for various signal-to-interference power ratio (SIR). The background noise power is set to be 3 dB lower than the desired signal power for this simulation to evaluate the interference-dominant condition. Interference packets have log-normal distribution with variance of 10 dB while their mean power is determined by SIR. The interference packets follow a Poisson arrival process with the mean interval of 5 ms (each interference packet is 2 ms long). Each sample in an interference packet is a i.i.d. Gaussian random variable (emulating OFDM). The desired HDM or BPSK-Polar signal has 1kHz bandwidth, thus each sample in the packet spans 1 ms. To increase the robustness to the outlier samples caused by strong short interference packets, HDM with L2-norm minimization sets a threshold of 2 (for I and Q each) to saturate the received signal amplitude. For the same reason, LLR is saturated at ± 5 for Polar decoding [18]. HDM does not use SI(N)R information for decoding while BPSK-Polar uses SNR information for LLR computation (using SINR degrades PER since interference is not AWGN).

Figure 3 confirms that HDM with L1-norm minimization yields the best performance. The HDM with L2-norm minimization also gives significantly (2.5dB SIR @ PER=10^{-3}) better performance than BPSK-Polar. It is because HDM is inherently more robust to interference due to sparse signal ($\mathbf{x}_i$) spreading via $\mathbf{A}_i$ [9]. Note that the gap between L1 and L2 minimization reduces as SIR increases, which is expected when interference no longer dominates.

Figure 4 shows the PER performance when interference packets have varying Poisson arrival rates. The SIR is set to -5 dB in this case. For a target PER of 10^{-2}, HDM with L1- and L2-norm minimization can operate in an environment with about $2\times$ and $1.5\times$ more frequent interference compared to BPSK-Polar, respectively.

To evaluate the performance in a realistic scenario, we use an USRP X310 to capture real interference packets from WiFi and Bluetooth. Captured spectrogram examples are shown in Figure 5. WiFi has 20MHz bandwidth while the Bluetooth has 2MHz bandwidth with frequency hopping. From the figure, one can observe that both WiFi and Bluetooth packets are about 2 ms long, which justifies our previous assumption.

We use the captured WiFi and Bluetooth traffic as the

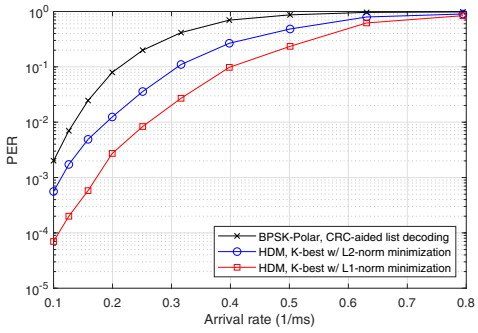

Fig. 4: PER in SIR = -5dB, varying arrival rates.

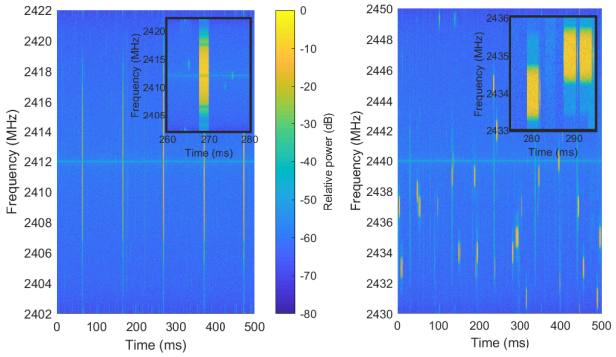

(a) WiFi (b) Bluetooth

Fig. 5: The interference spectrogram capture from ISM band.

interference source to simulate the PER performance under that scenario. To emulate heavy interference traffic, we overlay captured interference on top of each other. We collect 50 seconds of wideband data and process them into 10^5 narrowband interference frames added to each HDM / BPSK-Polar packet.

Figure 6 shows the PER performance under aforementioned setting. The SIR in x-axis is the ratio between the desired signal and the average (including idle time) power of the entire interference signal. The performance follows what we observed in simulated interference cases. As the PER is interference-limited, the HDM with L1 minimization method exhibits a large gain over the other schemes.

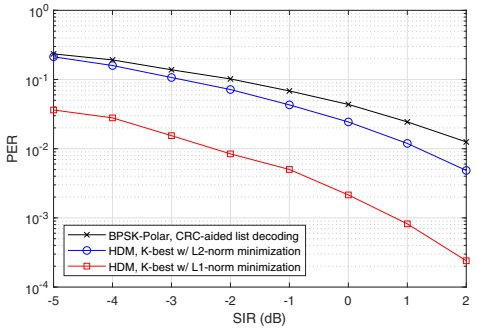

Fig. 6: PER with captured ISM band interference traffic.

VI. Conclusion

In this paper, we proposed a novel K-best CRC-aided decoding algorithm for HDM. The proposed algorithm has superior PER performance in AWGN compared to a state-of-the-art Polar code when packet length is short. Furthermore, we proposed an L1-norm based modified HDM decoding algorithm to boost the performance in interference-limited environments. Simulations with realistic interference show that the proposed HDM with L2 and L1 minimization provides superior PER performance in interference-limited scenarios.

Acknowledgement

This work was funded in part by DARPA YFA #D18AP00076 and NSF CAREER #1942806.

References

[1] "IMT vision—Framework and overall objectives of the future development of IMT for 2020 and beyond," *Int. Telecommun. Union, Geneva, Switzerland, ITU-Recommendation M.2083-0*, Sep 2016.

[2] Z. Dawy, W. Saad, A. Ghosh, J. G. Andrews, and E. Yaacoub, "Toward Massive Machine Type Cellular Communications," *IEEE Wireless Communications*, vol. 24, pp. 120–128, 2017.

[3] C. Bockelmann, N. Pratas, H. Nikopour, K. Au, T. Svensson, C. Stefanovic, P. Popovski, and A. Dekorsy, "Massive machine-type communications in 5g: physical and MAC-layer solutions," *IEEE Commun. Mag.*, vol. 54, no. 9, pp. 59–65, 2016.

[4] G. Durisi, T. Koch, and P. Popovski, "Toward Massive, Ultrareliable, and Low-Latency Wireless Communication With Short Packets," *Proceedings of the IEEE*, vol. 104, no. 9, pp. 1711–1726, 2016.

[5] Y. Polyanskiy, H. V. Poor, and S. Verdu, "Channel Coding Rate in the Finite Blocklength Regime," *IEEE Trans. Inf. Theory*, vol. 56, no. 5, pp. 2307–2359, 2010.

[6] L. Gaudio, T. Ninacs, T. Jerkovits, and G. Liva, "On the Performance of Short Tail-Biting Convolutional Codes for Ultra-Reliable Communications," in *SCC 2017; 11th International ITG Conference on Systems, Communications and Coding*, 2017, pp. 1–6.

[7] M. Baldi, F. Chiaraluce, N. Maturo, G. Liva, and E. Paolini, "A Hybrid Decoding Scheme for Short Non-Binary LDPC Codes," *IEEE Commun. Lett.*, vol. 18, no. 12, pp. 2093–2096, 2014.

[8] H. Kim, "HDM: Hyper-Dimensional Modulation for Robust Low-Power Communications," in *2018 IEEE International Conference on Communications (ICC)*, May 2018, pp. 1–6.

[9] C. Hsu and H. Kim, "Collision-Tolerant Narrowband Communication Using Non-Orthogonal Modulation and Multiple Access," in *2019 IEEE Global Communications Conference (GLOBECOM)*, 2019, pp. 1–6.

[10] I. Tal and A. Vardy, "List Decoding of Polar Codes," *IEEE Trans. Inf. Theory*, vol. 61, no. 5, pp. 2213–2226, 2015.

[11] M. C. Coşkun, G. Durisi, T. Jerkovits, G. Liva, W. Ryan, B. Stein, and F. Steiner, "Efficient error-correcting codes in the short blocklength regime," *Physical Communication*, vol. 34, pp. 66 – 79, 2019.

[12] R. Abbas, M. Shirvanimoghaddam, Y. Li, and B. Vucetic, "A Novel Analytical Framework for Massive Grant-Free NOMA," *IEEE Trans. Commun.*, vol. 67, no. 3, pp. 2436–2449, 2019.

[13] H. Ji and B. Shim, "Sparse Vector Coding for Short Packet Transmission in Massive Machine Type Communications," in *2018 24th Asia-Pacific Conference on Communications (APCC)*, 2018, pp. 137–140.

[14] A. Joseph and A. R. Barron, "Fast Sparse Superposition Codes Have Near Exponential Error Probability for $R < C$," *IEEE Trans. Inf. Theory*, vol. 60, no. 2, pp. 919–942, 2014.

[15] Zhan Guo and P. Nilsson, "Algorithm and implementation of the K-best sphere decoding for MIMO detection," *IEEE J. Sel. Areas Commun.*, vol. 24, no. 3, pp. 491–503, 2006.

[16] G. T. 38.212, "NR; Multiplexing and channel coding (Release 15)," *3rd Generation Partnership Project*, 2018.

[17] A. Goldsmith, *Wireless Communications*. Cambridge Univ. Press, 2005.

[18] M. Mehrnoush and S. Roy, "Coexistence of WLAN Network With Radar: Detection and Interference Mitigation," *IEEE Trans. on Cogn. Commun. Netw.*, vol. 3, no. 4, pp. 655–667, 2017.